Cold Regions Science and Technology 120 (2015) 45–55

Contents lists available at ScienceDirect

Cold Regions Science and Technology

journal homepage: www.elsevier.com/locate/coldregions

Measurements of the evolution of frazil ice particle size distributions

Vincent McFarlane, Mark Loewen *, Faye Hicks

University of Alberta, Department of Civil and Environmental Engineering, Edmonton, AB, Canada

ARTICLE INFO

Article history:
Received 15 July 2015
Received in revised form 1 September 2015
Accepted 1 September 2015
Available online 7 September 2015

Keywords:
Frazil ice
Turbulence
River ice processes

ABSTRACT

A series of 27 experiments were carried out at three different turbulence intensities in the frazil ice production tank at the University of Alberta. The frazil particles produced were photographed in suspension throughout the duration of the supercooling process using a high-resolution digital camera. An acoustic Doppler velocimeter (ADV) was used to record vertical profiles of the velocities at three locations in the tank, and the velocity time series data were processed to determine the rate of dissipation of turbulent kinetic energy per unit mass. A computer algorithm was written to process the captured images to determine the particle sizes and compute the properties of the particle size distribution. The resulting data were used to study the evolution of the size distribution throughout the supercooling process. It was found that the number of individual particles in suspension peaked shortly after the maximum degree of supercooling had been reached, and at approximately the same time the mean and standard deviation of the particle diameter approached constant values. The overall mean particle diameter prior to the onset of particle flocculation was found to decrease with increasing values of the dissipation rate, and ranged from 0.94 to 0.66 mm for dissipation rates of 24 to 336 cm^2/s^3.

1. Introduction

Frazil ice particles are formed in turbulent river flows when the water temperature has supercooled to a few one-hundredths of a degree below 0 °C. Suspended frazil particles exhibit a highly adhesive behaviour in supercooled water. This 'active' frazil readily freezes onto other frazil particles (forming flocs), to the streambed (forming anchor ice), and to man-made structures, such as trash racks on water intakes. As a result, active frazil can cause a number of problems. Large accumulations formed on trash racks can, in extreme cases, entirely block the flow into water intakes (Richard and Morse, 2008). Anchor ice can drastically alter the river geomorphology by raising the bed level, reducing the effective flow area, and forming anchor ice dams, all of which severely impact fish habitat (e.g. Stickler et al., 2010; Brown et al., 2011).

The supercooling process that initiates frazil ice production is well understood and has been documented thoroughly in previous studies (e.g. Carstens, 1966; Osterkamp, 1978; Tsang and Hanley, 1985; Clark and Doering, 2009). During a typical supercooling event, assuming the heat loss from the water surface to the air above is constant, the water temperature initially decreases at a nearly constant rate. Shortly after the water temperature drops below 0 °C, frazil ice crystals begin to form and release latent heat into the flow. As more and more crystals are produced, the amount of latent heat released becomes increasingly significant, decreasing the cooling rate until the maximum degree of supercooling is reached, and the water temperature then begins to increase (Daly, 2013). Eventually a point in time is reached where the amount of heat lost to the cool air and the amount of heat gained from ice formation are in equilibrium, and the water temperature levels off at a 'residual' supercooled temperature. The period of time between when the water first drops below 0 °C and when the residual temperature is reached is called the period of 'principal supercooling' (Ye et al., 2004). During this time period the size distribution of suspended frazil particles is constantly evolving due to the processes of particle formation, growth, and flocculation (Ye et al., 2004). The earliest particles are generally formed from small ice nuclei (e.g. snow flakes, frost, fragments of border or skim ice), which then increase in diameter (Daly, 2013). These larger particles collide either with each other or the riverbed and banks causing small ice nuclei to break free and form new, small crystals in a process known as 'secondary nucleation' (Daly, 2013). Active frazil ice particles are removed from suspension when they collide and freeze together forming frazil flocs which rise to the surface once they are large enough to overcome the turbulence in the flow (Daly, 2013).

Much of what is known about the characteristics of frazil ice has been determined from laboratory experiments. This is due to the difficulties presented by the small size, non-spherical shape, and optical properties of frazil ice, as well as the challenges of performing winter field work on rivers (Daly, 1994). Some photographs of suspended frazil ice particles in natural streams have been reported (Osterkamp and Gosink, 1983; Dubé et al., 2014), and the use of acoustic devices has proven to be a promising method for estimating concentrations and size distributions of particles in the field (e.g. Marko et al., 2015;

* Corresponding author at: Water Resources Engineering, 7-289 Donadeo Innovation Centre for Engineering, University of Alberta, Edmonton, Alberta, T6G 2W2, Canada. Tel.: +1 780 9778883.

E-mail addresses: vmcfarla@ualberta.ca (V. McFarlane), mrloewen@ualberta.ca (M. Loewen), fhicks@ualberta.ca (F. Hicks).

http://dx.doi.org/10.1016/j.coldregions.2015.09.001
0165-232X/

Ghobrial et al., 2013; Jasek et al., 2011; Morse and Richard, 2009; Richard et al., 2011), but quantitative field measurements of frazil ice properties remain very scarce.

The purpose of this study was to investigate how the size distribution of suspended frazil particles evolves throughout a supercooling event, and to explore the effects of increasing turbulence intensity on this process. A series of laboratory experiments were performed in a frazil ice tank at various turbulence intensities to examine this, and particle sizes were measured from high-resolution digital images. The use of high-resolution digital cameras allowed for the inclusion of very small particles in calculating the size distribution.

2. Literature review

Individual frazil particles measured in laboratory environments are predominately disc-shaped and have been observed to have diameters in the range of 23 μm to 5 mm in the past, with size distributions in most cases well described by a lognormal distribution (e.g. Clark and Doering, 2008 2006,; Daly and Colbeck, 1986; Doering and Morris, 2003; Ghobrial et al., 2012; Gosink and Osterkamp, 1983; McFarlane, 2014; Ye et al., 2004). However, the minimums, maximums, means, and standard deviations of the particle diameters have been different in all of these studies. There are many possible factors that have contributed to these differences. Daly and Colbeck (1986), for example, observed particles ranging in diameter from about 35 μm to 0.5 mm using a 35 mm camera-microscope system and reported mean diameters "generally above 0.1 mm." Daly and Colbeck (1986) also reported particle concentrations ranging from 0.17 to 0.982 particles/cm^3. However, their frazil particles were produced in a 36.6 m long flume and consequently the particles may not have had sufficient time to grow to larger diameters before the water was recirculated and the existing particles were melted out. Alternatively, the counter-rotating flume used by researchers at the University of Manitoba (e.g. Doering and Morris, 2003; Ye and Doering, 2004; Ye et al., 2004; Clark and Doering, 2009, 2008, 2006) allowed frazil particles to continue to seed, develop, and flocculate over the course of an experiment, enabling larger particles to develop and be observed. As a result larger mean particle sizes were observed in these studies (e.g. 0.79 to 1.58 mm by Clark and Doering (2008)). However, these measurements were limited by the resolution of the digital cameras used, which resulted in a minimum observable particle size of ~0.2 mm.

The differences between the measured particle sizes in past experimental studies may also be due to the influence of flow characteristics such as turbulence intensity on the development of frazil ice particles. Understanding these influences may be instrumental in improving our understanding of how frazil particles behave in natural river flows, which are much less predictable than laboratory environments. A few studies have measured the impact of different turbulence parameters on frazil size. Ettema et al. (1984) produced frazil ice particles in a mixing jar and used an oscillating grid to vary the turbulence intensity. In this way, flows were produced with values of the turbulence exchange coefficient ranging from approximately 6 to 19 cm^2/s and an overall trend of decreasing frazil 'platelet' (i.e. floc) size with increasing turbulence intensity was observed.

Ye et al. (2004) produced frazil ice particles in a counter-rotating flume at various air temperatures and water velocities and studied the impact of these variables on the supercooling process and mean particle size. In these experiments, Ye et al. (2004) observed that the frazil particles increased in number and mean diameter during the period of principal supercooling, and that the mean diameter reached a stable value (termed D_{50sp}) once the principal supercooling period had ended, while the number of observed particles dropped off. Ye et al. (2004) also compared the values of D_{50sp} to the Reynolds number of the flow, and found that the mean frazil diameter at the end of the principal supercooling period increased with an increasing Reynolds number.

Clark and Doering (2008) carried out a study specifically focusing on the effects of turbulence intensity on frazil ice particles in the same counter-rotating flume. By fitting the flume with bed plates of varying roughness they were able to vary the dissipation rate of turbulent kinetic energy per unit mass in the flow, ε, from about 113 to 1496 cm^2/s^3. After calculating the size distributions of the observed particles for each of these flows, Clark and Doering (2008) observed that both the mean and standard deviation of the particle diameters first increased with increasing values of ε up to about 900 cm^2/s^3, and then decreased. For both the mean and standard deviations these relationships were well described by parabolic functions. Similar to Ye et al. (2004), they also observed that the number of clear, disc-shaped particles in the flow increased during the period of principal supercooling and decreased thereafter.

The results obtained by Clark and Doering (2008) and Ye et al. (2004) support the theoretical analysis presented by Daly (2013, 1994, 1984) who suggested that the limiting factor in the growth rate of a frazil particle's diameter is the rate at which the latent heat released by crystallisation can be advected away from the crystal by the flow. This means that, as the turbulence intensity increases, the frazil particles in the flow would be able to grow more quickly and, presumably, to a larger crystal diameter. However, increased turbulence intensity could also cause an increase in the number of crystal collisions, and it was hypothesised by Clark and Doering (2008) that there might be a point at which increasing turbulence intensity actually results in eddies that are strong enough to overcome the weak mechanical strength of frazil crystals. This would result in particle fracture and thereby physically limit the average particle size. Both of these processes would result in increased secondary nucleation. Daly (2013) noted that this would lead in a relatively large number of small frazil crystals being produced at high turbulence levels, and this could explain the decrease in mean particle size that Clark and Doering (2008) observed for dissipation rates greater than about 900 cm^2/s^3.

3. Experimental set-up

Experiments were performed in the University of Alberta's Civil Engineering Cold Room Facility using a frazil ice production tank (illustrated in Fig. 1) with base dimensions of 0.8 by 1.2 m and filled to a depth of 1.3 m with filtered tap water. During experiments, turbulence in the tank was generated by four variable speed propellers powered by NEMA 34 DC variable speed electric motors (278 W, 1.514 N-m of torque, max speed 1750 rpm) and mounted on the bottom of the tank. The frazil ice particles were illuminated using two arrays of Larson Electronics 24-bulb, 3-W light-emitting diode (LED) lights that were mounted against the back glass wall of the tank and diffused by translucent plastic sheeting. Directly opposite the lights, two Cavision 10 cm square glass polarising filters were mounted in the tank flush to the front glass wall. These polarisers were mounted parallel to each other and spaced 2.2 cm apart, with one of them rotated 90° with respect to the other, to cross-polarise the light passing through them. This achieved the effect of producing a black background in the captured images where only the ice particles passing between them, that had refracted the incident light, were visible. A Sea-Bird SBE 39 temperature recorder (accuracy ±0.002 °C) was used to record the water temperature throughout the experiments and was connected to a computer located outside the cold room to allow for real-time monitoring of the supercooling process. The temperature recorder was placed in an approximately symmetrical location and at a comparable depth to the polarisers. This was to avoid interfering with the flow through the measuring volume while still providing a representative temperature to where the frazil particle images were captured.

The camera used for the experiments was a Nikon D800 digital single-lens reflex (DSLR) equipped with a Kenko 25 mm Uniplus Tube DG extension ring and an AF Micro-Nikkor 60 mm f/2.8D lens. The Nikon D800 has a 36 megapixel resolution and, when used with the

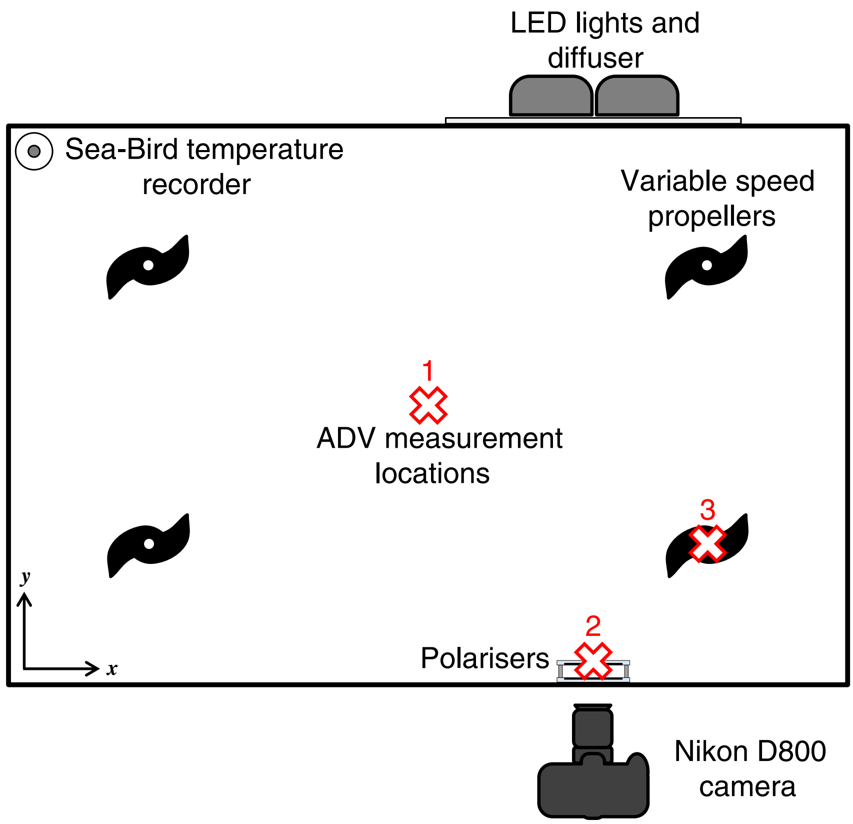

Fig. 1. Plan view of the frazil ice tank showing the locations of the camera, LED lights, polarisers, four propellers, and the three locations where the ADV measurements were made (marked by the red X's). The coordinate system for the ADV measurements is defined such that the positive *x* and *y*-directions are towards the right and back of the tank, respectively, and the positive *z*-direction is towards the water surface.

macro lens and extension tube, the average pixel size in the images was ~5.6 μm, allowing very small particles to be resolved in the images. This resulted in an average measuring volume of 24.6×10^{-6} m^3 in the experiments. During a series of preliminary experiments, the aperture, shutter speed, and ISO settings of the camera were tested, and settings of f/25, 1/2000s, and ISO 6400 were determined to offer the best balance of depth of field and brightness with minimal background noise.

Velocity time series measurements were recorded in the tank using a Nortek Vectrino acoustic Doppler velocimeter (ADV) mounted on a frame above the tank that allowed it to be positioned to record a vertical profile anywhere in the tank. The ADV could be positioned at depths ranging from the bottom of the tank up to a depth of about 240 mm below the water surface, due to the limited clearance above the tank in the cold room.

4. Experimental procedure

At the start of each experiment the four propellers located at the bottom of the tank were set to the desired speed (125, 225, or 325 rpm), verified using a laser tachometer. The temperature recorder mounted in the tank was programmed to begin recording the water temperature and the air temperature in the cold room was reduced from 2 °C to −10 °C over approximately 2 to 3 min. Images were then captured of a clear plastic ruler positioned at the front, back, and mid-point between the polarisers, both to focus the camera and to provide a scale for processing the frazil images. When the water temperature reached 0 °C, the camera was manually activated to record images at a rate of 1 Hz for a duration of 999 s. Once the camera had finished capturing images, the propellers were switched off and the temperature in the cold room was raised to 2 °C to allow the ice to melt prior to the next experiment.

Measurements of the turbulent velocities were made using the Vectrino ADV in separate experiments while the water temperature was held constant at approximately 2 °C. At each of the three propeller speeds, ADV measurements were made at nine depths at the three locations shown in Fig. 1; at the centre of the tank, near the front glass wall where the polarisers were placed when collecting images, and directly above one of the propellers. These locations were selected to provide a representative sample of the turbulence characteristics throughout the tank. At the propeller speeds of 125 and 225 rpm velocity measurements were taken at a sampling frequency of 50 Hz for a duration of 5 min and, for the speed of 325 rpm, a frequency of 100 Hz was used for the same duration.

5. Data analysis

5.1. ADV data

The ADV data were analysed using a Matlab program. The first step in the analysis was the application of the despiking algorithm developed by Islam and Zhu (2013) to the raw ADV data files. This despiking method was selected because it has been demonstrated to be effective at removing spikes from data contaminated by up to 70% spikes (Islam and Zhu, 2013). This method was applicable because up to 32.5% spikes were observed in the velocity time series data from the frazil ice tank. Next, the despiked time series data were corrected for Doppler noise using the method developed by Romagnoli et al. (2012) and decomposed into mean and turbulent velocity components. The decomposed data were then used to compute a variety of turbulence characteristics at each measurement point in the tank. In particular, frequency spectra computed from the despiked time series were plotted and the minimum and maximum frequencies for the range of frequencies within the inertial subrange were determined (i.e. frequencies where a slope of −5/3 occurred). This region of the frequency spectrum was then used to calculate the turbulent kinetic energy dissipation rate per unit mass at each location for each propeller speed (Tennekes and Lumley, 1972). Taylor's 'frozen turbulence' hypothesis was used in calculating the dissipation rates from the frequency spectra, which requires the assumption that the turbulent structures do not change appreciably in the time it takes for them to be advected past the point of measurement (Stiansen and Sundby, 2001). The equation used was:

$$\varepsilon = 2\pi\left(\frac{P_i f^{5/3}}{A U_i^{2/3}}\right)^{3/2} \qquad [1]$$

where ε is the dissipation rate of turbulent kinetic energy per unit mass (m^2/s^3); P_i is the power spectral density in direction i (m^2/s); f is the frequency (Hz); A is a constant taken to equal 0.49 (Pope, 2000); and U_i is the convective velocity in direction I (m/s). Stiansen and Sundby (2001) provide a detailed discussion and comparison of this, and other, methods for calculating the dissipation rate from the frequency spectra. A block width of 512 with a 50% overlap was used in calculating the frequency spectra, giving a normalised random error of ±13% for the 125 and 225 rpm propeller speeds (50 Hz sampling rate) and ±9% for the 325 rpm propeller speed (100 Hz sampling rate). A typical frequency spectrum fitted with the −5/3 slope is shown plotted in Fig. 2.

In Fig. 3 the dissipation rate, ε, is plotted versus the water depth at the measurement location directly above the one propeller, and can be seen to increase up to a depth of 825 mm for the w-component and 925 mm for the u- and v-components. The 1025 mm measurement, which was taken approximately 85 mm above the propeller, was the smallest by a significant amount in all cases. These small values are likely caused by the presence of very high shear close to the propeller that results in unreliable ADV velocity measurements (McLelland and Nicholas, 2000). Therefore, the dissipation rate estimates at the 1025 mm depth were omitted when depth-averaging the dissipation rates above the propeller and, to be consistent, at the other two vertical profile locations as well. The depth-averaged values of the dissipation rate computed from the three velocity components at each location, and for all propeller speeds, are presented in Table 1.

Examination of the depth-averaged values in Table 1 and the data plotted in Fig. 3 shows that the dissipation rates estimated from the u and v velocity components were comparable, while the w-component value tended to be about an order of magnitude smaller. The reason

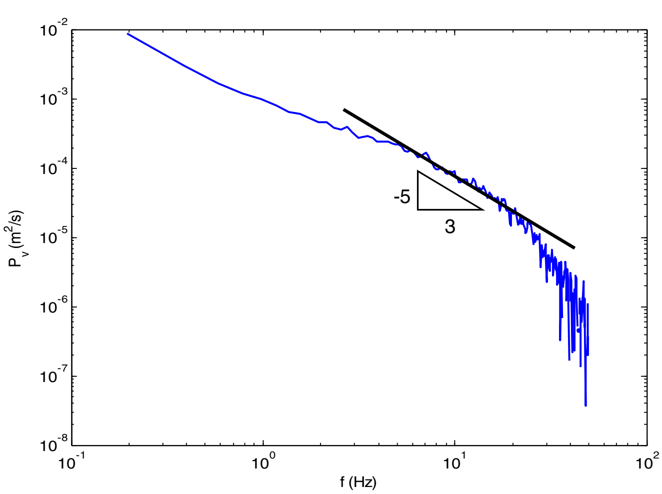

Fig. 2. Power spectra calculated for the 325 rpm propeller speed in the centre of the tank at a depth of 625 mm. P_v is the value of the power spectral density (m^2/s) in the y-direction and f is the frequency (Hz). A line with a slope of −5/3 is shown over the region determined to be the inertial subrange, used to calculate the dissipation rate of the turbulent kinetic energy.

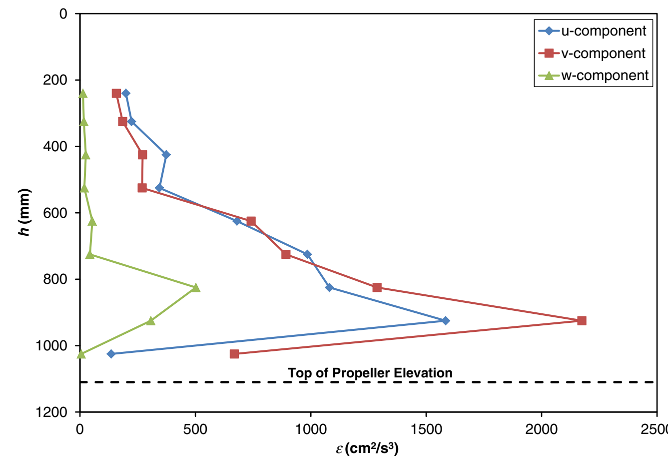

Fig. 3. Turbulent kinetic energy dissipation rate (ε) throughout the water depth (h), measured above the propeller for a speed of 325 rpm. The u, v, and w-components represent the x, y, and z-directions, respectively.

for this discrepancy was investigated but no satisfactory explanation was found. The data in Table 1 also show that, as expected, the dissipation rate varies spatially in the tank and is highest directly over the propellers. Tank-averaged estimates of ε were calculated using the values computed from the u and v-components, which were then averaged spatially over the three measurement locations. This results in values of 23.9, 85.5, and 336 cm^2/s^3 for propeller speeds of 125, 225, and 325 rpm, respectively. Note that if the dissipation estimates computed from the w-component are included when calculating tank-averaged values this reduces the magnitude by only ~30%, and such a reduction would not alter any of the conclusions drawn from this study.

Determining how comparable the rates of dissipation in the tank are to those observed in natural rivers would be quite useful. However, an extensive literature search did not find any dissipation rates measured in rivers for comparison. As an alternative, estimates of the dissipation rates in a number of natural rivers in the Alberta were calculated using the average channel slopes, velocities, depths, and widths reported by Kellerhals et al. (1972) using the following equations:

$$u_* = \sqrt{gR_hS} \qquad [2]$$

$$\varepsilon = \frac{u_*^3}{\kappa R_h}\left[\ln\left(\frac{u_*R_h}{\nu}\right) - 1\right] \qquad [3]$$

where u^* is the shear velocity (m/s); R_h is the hydraulic radius (m), calculated based on the average channel depth and width; g is the acceleration due to gravity, taken to equal 9.81 m/s^2; κ is von Karman's constant, taken to be 0.4; and ν is the kinematic viscosity of water, taken to equal 1.8×10^{-6} m^2/s for water at 0 °C (Clark and Doering, 2008). Kellerhals et al. (1972) reported 359 depth, width, slope, and velocity values for 54 different rivers, and using Eqs. (2) and (3) dissipation rates were predicted to range from 4.2 to 14,968 cm^2/s^3, with an average of 1164 cm^2/s^3. A total of 210 of these 359 estimates (58%) fell within the same range as the u and v-component depth-averaged dissipation rates obtained in this study (Table 1), indicating that the strength of the turbulent mixing in the tank was comparable to that in natural streams.

5.2. Frazil images

A typical cross-polarised digital image of frazil ice particles is shown in Fig. 4. The digital images were processed using a Matlab algorithm that was written to identify and compute the size of each individual frazil particle. The algorithm first loaded a 'raw' image and then subtracted a background image (i.e. an image captured prior to the formation of any ice in the tank) from it, to remove any of the imperfections visible in all of the

Table 1
Depth-averaged values of the turbulent kinetic energy dissipation rate per unit mass, ε (cm^2/s^3) for each velocity component, propeller speed, and vertical profile location.

Velocity component	125 rpm			225 rpm			325 rpm		
	Centre	Glass	Propeller	Centre	Glass	Propeller	Centre	Glass	Propeller
u	11.4	10.1	66.6	41.9	30.7	174.2	167.3	159.2	684.1
v	8.1	6.7	40.3	30.9	26.8	208.6	138.2	117.8	747.4
w	0.7	0.6	3.1	2.6	2.3	18.0	10.7	8.6	122.6
u–v average	9.7	8.4	53.5	36.4	28.8	191.4	152.7	138.5	715.7

images (e.g. spots on the lens, scratches on the glass, etc.). Second, the resulting image was converted into high-threshold and low-threshold binary images. The two binary images were then compared to each other using an iterative dilation and erosion procedure, until the extent of each individual particle had been determined. Next, the area and perimeter of each particle in the final binary image were compared to the area and perimeter of a fitted ellipse, since most frazil particles are expected to be disc-shaped. If the area and perimeter of the particle were similar enough to those of the fitted ellipse, then the particle was identified as a frazil ice particle and included in the data set used to calculate the properties of the size distribution. Approximately 75% of the particles identified were confirmed to be disc-shaped using this test, and by manually checking nearly 1000 particles it was determined that the particles were correctly identified as being disc-shaped or not, more than 93% of the time. This test not only ensured that irregularly shaped individual particles were excluded; it also rejected any frazil flocs that appeared in the images. Finally, the diameter of each confirmed frazil particle was calculated and the properties of the resultant size distribution for the entire image series, including the mean, median, and standard deviation, were computed. As mentioned in Section 2, a lognormal distribution has been observed to fit the size distribution of frazil particles in the past. With this in mind, a lognormal distribution with the same mean and standard deviation as the measured data was calculated for each experiment and plotted along with the observed size distribution for comparison. An example size distribution for a single experiment is shown in Fig. 5 along with the computed lognormal distribution.

After computing the particle sizes for each individual experiment it was desirable to combine the data from each experiment (i.e. ensemble average) at each propeller speed in order to observe how the particle characteristics evolved with time. There were 10 experiments processed for the 125 rpm propeller speed, five for 225 rpm, and 12 for 325 rpm. The repeatability of the experiments at each propeller speed was assessed by comparing supercooling curves that were synchronised to the time at which the temperature reached 0 °C. A plot showing the superimposed supercooling curves for the 12 experiments conducted at 325 rpm is presented in Fig. 6. This plot shows that the rate of cooling (i.e. the slope of the curves from 0 to about 400 s) and the residual supercooling temperatures did not vary significantly (e.g. the cooling rate varied from 0.012 to 0.015 °C/min over the 12 experiments). This demonstrates that the cold room temperatures were being varied in a controlled manner and that the supercooling process was repeatable. However, significant variations were observed in the minimum temperature, which varied from −0.093 °C to −0.072 °C, and in the duration of the principal supercooling period, which varied from approximately 12 to 15 min. These variations may have been caused by variations in the seeding rate; that is, the rate at which ice crystals were introduced into the supercooled water from the air in the cold room. Model simulations by Hammar and Shen (1995) have shown that varying the seeding rate will produce variations in the supercooling curve very similar to those observed in Fig. 6 (see their Fig.3). The most likely source of seed particles is the frost that forms in the cold room refrigeration system when warm air is cooled. These ice crystals enter the cold room via two large cold air vents mounted in the ceiling and the rate at which they seed the supercooled water in the tank would be expected to vary from one experiment to the next due to a variety of factors. Despite the variations in the supercooling curves that were observed, the experiments were judged to be sufficiently repeatable that the data could be ensemble-averaged at each of the three propeller speeds.

6. Results and discussion

6.1. Evolution of size distribution

In order to observe how the particle properties changed throughout the supercooling process, the experiments for each propeller speed were synchronised using the time at which the minimum temperature

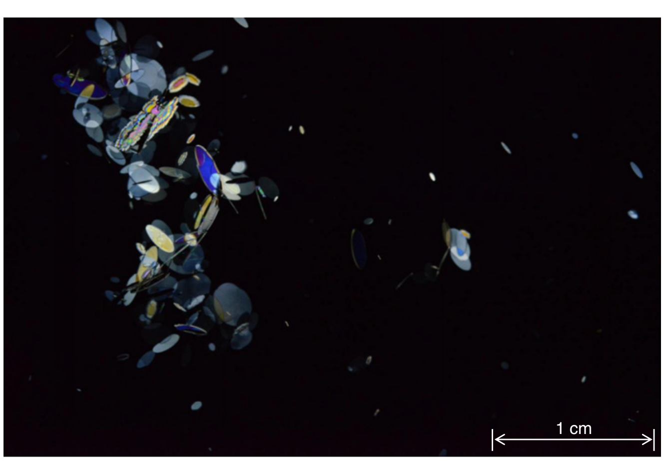

Fig. 4. A sample unprocessed image, captured during one of the 225 rpm experiments, showing individual particles and a small frazil floc. The spacing between the polarisers was 2.2 cm.

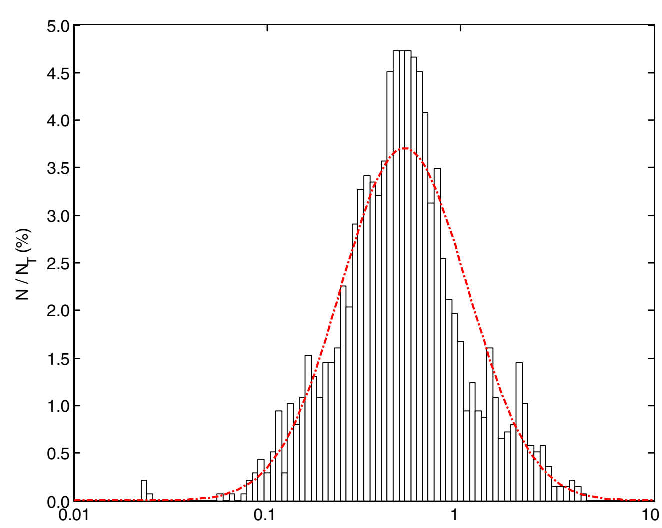

Fig. 5. Size distribution for particles observed prior to flocculation for an experiment carried out at a propeller speed of 325 rpm. N is the number of particles in each bin, N_T is the total number of particles, and D is the diameter. The dot-dash line is the corresponding ideal lognormal distribution.

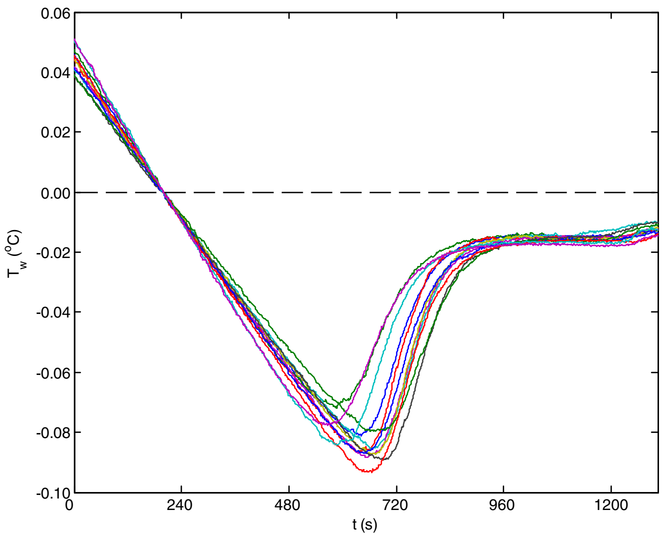

Fig. 6. Superimposed supercooling curves showing the water temperature, T_w, as a function of time, t, for the 325 rpm experiments.

was reached. The supercooling curve was then ensemble-averaged across all of the experiments and a 5 point median filter was applied to remove random noise (Pratt, 2007). In Fig. 7, the time series of the 35 s moving mean, standard deviation, and number of observed particles are plotted for the 325 rpm experiments. By recording these three parameters, it is possible to plot a theoretical distribution at any point in time that approximates the size distribution of the observed frazil particles. Note that the mean and standard deviation plots begin later than the plot of the number of particles because these two parameters were only calculated when a minimum of ten particles were available for averaging.

First, examining the number of observed particles (Fig. 7a), it is clear that the number of particles increased quite rapidly at a fairly constant rate until just after the maximum supercooling had been reached, achieving an ensemble-averaged peak number concentration of 1.8 particles/cm^3 in the sampling volume of 24.6 cm^3. This is logical, as the rapid increase in the number of frazil particles suspended in the water results in a large release of latent heat due to crystallisation, causing the water temperature to increase. The higher concentration of frazil particles also leads to an increased likelihood of particle collisions which has two potential effects: 1) increasing the number of small particles produced due to particle fracture and secondary nucleation, and 2) increasing the size and/or number of frazil flocs. As more and more particles flocculate and rise to the surface, the number of individual particles in suspension begins to decrease, and this can be seen as the number of particles decreases steadily when the water reaches the residual supercooling temperature. This is the same trend that was observed by both Ye et al. (2004) and Clark and Doering (2009, 2008, 2006).

In Fig. 7b it is seen that the moving average particle diameter follows a similar trend as the number of suspended particles. Although the peak

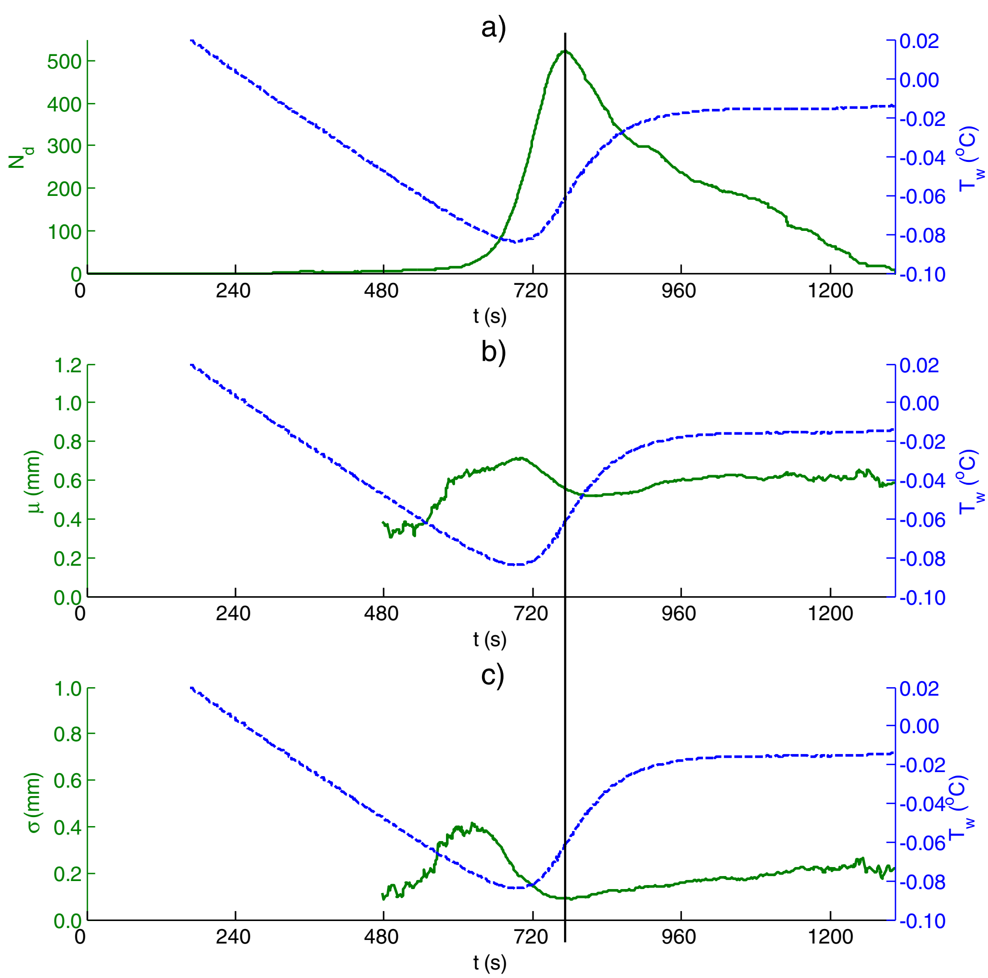

Fig. 7. Time series of the 35 s moving average particle properties for the twelve 325 rpm experiments plotted along with the ensemble-averaged supercooling curve, T_w (dashed line). a) N_d, the average number of particles observed in the 35 s window and summed over the 12 experiments, b) the mean particle diameter, μ, and c) the standard deviation, σ. The black vertical line indicates the time at which the maximum number of particles were observed.

is not quite as pronounced, the mean particle size is relatively small when there are few particles in suspension (~0.35 mm at 480 s), slowly increases to a maximum as more and more particles are produced (~0.7 mm at 700 s), begins to decrease as the maximum number of particles is approached, and levels off to a relatively constant size once the number of particles begins to decrease (~0.6 mm at 930 s). The decrease in mean particle size is caused by some combination of an increase in the number of smaller particles and a decrease in the number of larger particles. However, considering that at the time that the mean approaches an equilibrium value, the number of particles suspended in the water is decreasing, it seems likely that the number of large particles is decreasing faster than the number of small particles is increasing. This would imply that the larger frazil particles are more prone to flocculation, or fracture, than smaller ones due to an increased probability of larger particles colliding. A similar trend is observed in the standard deviation time series in Fig. 7c, which begins at ~0.1 mm at 480 s and peaks at ~0.4 mm at 620 s, although the decrease occurs approximately 80 s earlier than that of the mean, and it continued to climb slowly for the remainder of the experiment.

Clark and Doering (2008) plotted the mean and standard deviation of their data in a similar manner, and the trend of an increase to a peak followed by a slow decrease to an equilibrium value is visible in some of their plots. However, their data were collected in bursts separated by 45 s and therefore it is possible that some of the temporal changes in the mean and standard deviation were not captured. This possibility was acknowledged by Clark and Doering (2008) when they noted that it was difficult to accurately resolve the variation of the mean and standard deviation owing to the small number of measurements recorded in the early stages of each experiment.

For comparison, the same time series plots are shown for the five 225 rpm experiments in Fig. 8. The trend for all three subplots is similar for the 325 and 225 rpm experiments with the main difference being that the number of particles does not increase nearly as rapidly in the 225 rpm case and does not reach as high of a value (e.g. ~44 particles per experiment in Fig. 7a but only ~24 particles per experiment in Fig. 8a). This resulted in a peak concentration of 1.0 particle/cm^3 on average in the 225 rpm case. Based on visual observations made during the experiments and confirmed by the images taken at each propeller speed, it is likely that the main reason for this is the amount of flocculation that occurred. While less time passed before flocculation was observed in the 325 rpm case, large flocs routinely became frozen to the polarisers during the 225 rpm experiments and had to be knocked loose. This was not a problem that was regularly encountered during either the 125 or 325 rpm experiments. Based on this information it appears that the turbulence characteristics of the 225 rpm case offered ideal conditions for allowing particles to flocculate and remain in suspension. The 325 rpm case produced the most particles and resulted in a large amount of flocculation, but the currents in the tank were strong enough to draw those flocs not buoyant enough to reach the surface down to the bottom, where they were shredded by the propellers, resulting in a large number of individual particles remaining in suspension. In the 125 rpm case, fewer particles were observed at any given

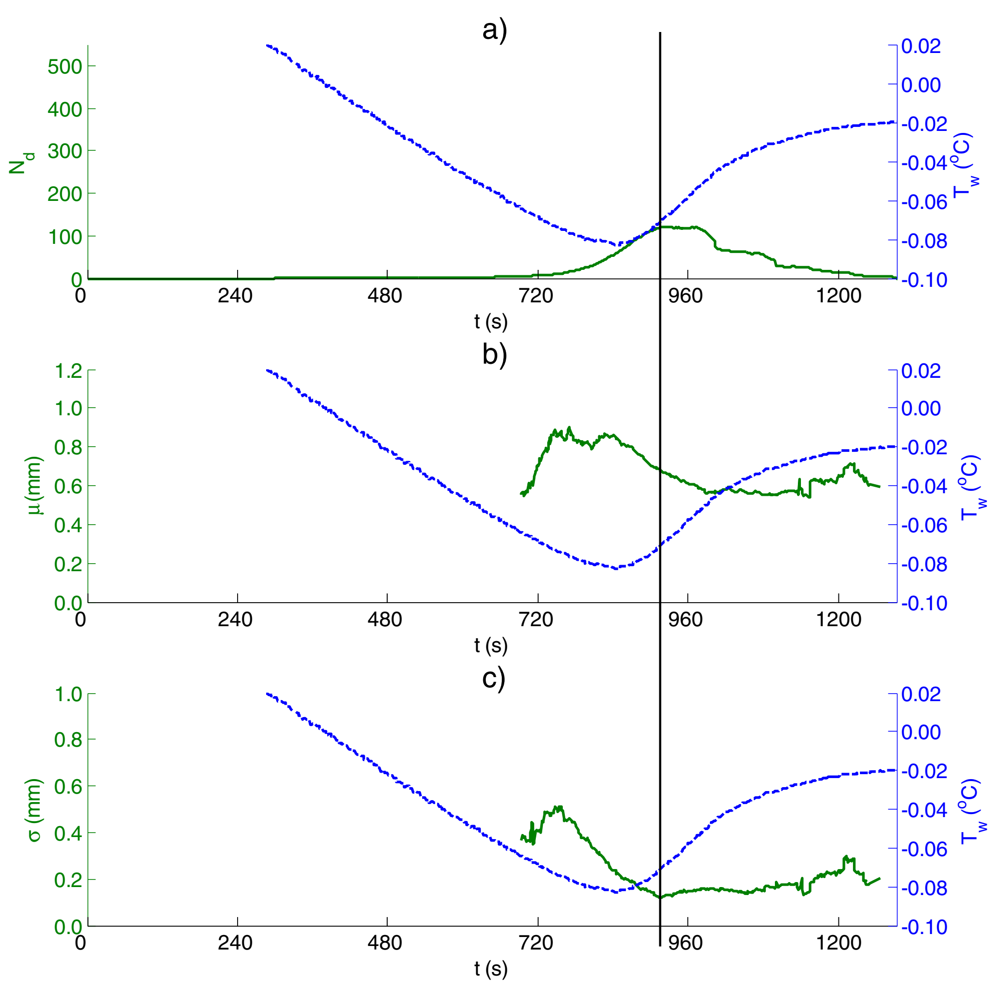

Fig. 8. Time series of the 35 s moving average particle properties for the five 225 rpm experiments plotted along with the ensemble-averaged supercooling curve, T_w (dashed line). a) N_d, the average number of particles observed in the 35 s window and summed over the 5 experiments, b) the mean particle diameter, μ, and c) the standard deviation, σ. The black vertical line indicates the time at which the maximum number of particles were observed.

time during an experiment, with a maximum concentration of 0.29 particle/cm^3 on average, which led to a decreased chance of flocculation occurring. Those flocs that did form were able to overcome the weaker currents in the tank and float up to the surface, resulting in few flocs appearing in the images or freezing onto the polarisers, but removing individual particles from suspension. It is of note that the peak concentrations observed in this study, which ranged from 0.29 to 1.8 particles/cm^3, are comparable to the concentrations of 0.17 to 0.982 particle/cm^3 reported by Daly and Colbeck (1986).

The growth rate and maximum achievable size of frazil ice particles have also been shown to be influenced by the concentration of particles in the flow and the level of supercooling (Forest, 1986; Forest and Sharma, 1992). As more and more frazil ice particles are produced, the concentration of dissolved solids in the supercooled water increases due to the rejection of these impurities from the frazil crystals, thereby reducing the freezing point of the water (Forest, 1986). Furthermore, the degree of supercooling of the water is reduced due to the latent heat released by ice formation, as already discussed. Forest (1986) and Forest and Sharma (1992) demonstrated that these two factors combine to slow down and eventually halt the growth of individual frazil particles even though the water surrounding them remains supercooled to a certain degree. This could be the reason the average particle diameter approaches a near-constant value once the residual supercooling temperature has been reached in Figs. 7b and 8b.

To better understand how the shape of the size distribution evolves and observe whether or not a lognormal distribution is an appropriate approximation at all stages of a supercooling event, the time series were broken up into three time intervals based on the peak number of particles observed in the ensemble-averaged data, following Clark and Doering (2006). Three intervals were defined based on the time at which number particles first reached 10% of the maximum, 90% of the maximum on either side of the peak, and when 30% of the maximum was observed on the subsequent decline, referred to as t_{10}, t_{90a}, t_{90b}, and t_{30}, respectively. The 'production' interval included all particles observed between t_{10} and t_{90a}, the 'peak' interval included all particles observed between t_{90a} and t_{90b}, and the 'flocculation' interval included all particles observed between t_{90b} and t_{30}. The size distributions in these three intervals and the distribution over the entire duration are plotted in Figs. 9 and 10 for the 325 and 125 rpm experiments, respectively. The distributions for the 225 rpm case, though not shown, were very similar. The mean diameter, standard deviation, and total number of frazil particles observed in each interval are listed in Table 2 for the three propeller speeds. In all plotted intervals the distribution shapes were very similar although the mean and standard deviation vary slightly, which can be seen clearly in Table 2. Also apparent in Fig. 9 is that the distributions seem to deviate from the ideal lognormal distribution and plateau at a diameter of approximately 2 mm. This was observed in all of the distributions at each propeller speed, and was most pronounced for the 125 rpm experiments where a secondary peak was visible between 2 and 3 mm. The reason for this is unknown; however, the lognormal curve does still represent the shape of the distributions reasonably well, and appears to be a suitable approximation for the size distribution of frazil ice particles at any point in the supercooling process.

6.2. Effect of turbulence

Across the 27 total experiments that were analysed, particles ranging in size from about 22 μm to 5.5 mm in diameter were observed. Only the 'pre-flocculation' images were used in calculating the size distributions for the suspended frazil particles to be compared to the turbulent kinetic energy dissipation rate. The images to be used in analyzing the effect of turbulence were determined for each experiment by noting the image in which small flocs (i.e. accumulations of 4 or more particles) appeared regularly. For the 325 rpm experiments this meant that ~350 images from each experiment were included in calculating the size distribution; for the 225 rpm experiments ~450 images were used; and for the 125 rpm experiments all 800 of the processed images were included. The means and standard deviations of the particle diameters obtained for each propeller speed after ensemble averaging, and the total number of detected frazil discs, are listed in Table 3.

It is clear from Table 3 that the mean particle size prior to flocculation decreased with increasing propeller speed, and therefore with

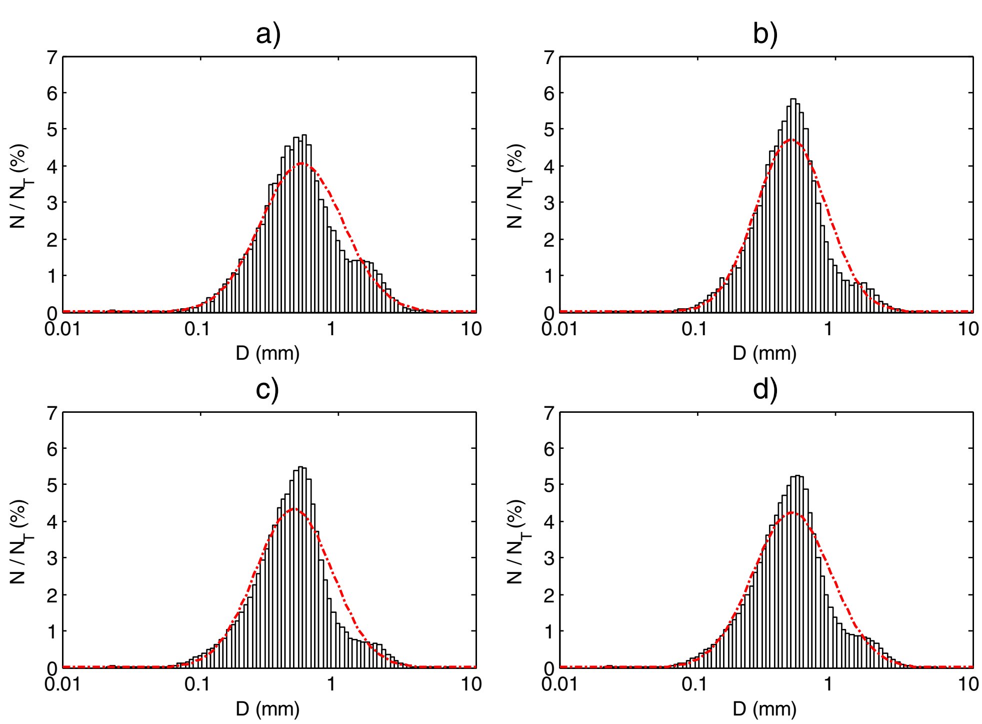

Fig. 9. Ensemble size distributions at the 325 rpm propeller speed for a) the production range (i.e. from t_{10} to t_{90a}), b) the peak range (i.e. between t_{90a} and t_{90b}), c) the flocculation range (i.e. between t_{90b} and t_{30}) and d) the entire data series. N is the number of particles in each bin, N_T is the total number of particles, and D is the diameter. The dot-dash lines are the corresponding lognormal distributions.

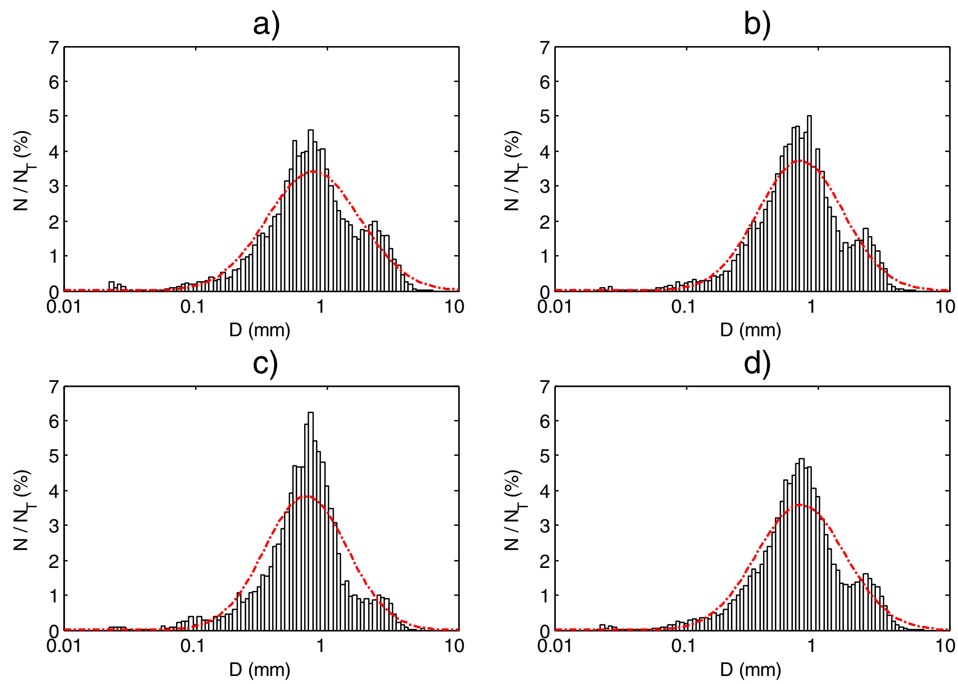

Fig. 10. Ensemble size distributions at the 125 rpm propeller speed for a) the production range (i.e. from t_{10} to t_{90a}), b) the peak range (i.e. between t_{90a} and t_{90b}), c) the flocculation range (i.e. between t_{90b} and t_{30}) and d) the entire data series. N is the number of particles in each bin, N_T is the total number of particles, and D is the diameter. The dot-dash lines are the corresponding lognormal distributions.

increasing turbulence intensity. In Fig. 11 the mean particle diameter prior to flocculation is plotted versus the mean depth-averaged dissipation rate (i.e. average of all three vertical profiles) as well as the maximum and minimum depth-averaged values for each propeller speed. At all three propeller speeds the minimum depth-averaged dissipation rate was observed near the glass and the maximum was observed directly over the propeller.

A power series regression was fitted to each relationship plotted in Fig. 11 and described the decrease in mean particle size very well, with an R^2 value greater than 0.94 in all three cases. This trend is contrary to the results obtained by Clark and Doering (2008) and Ye et al. (2004). Specifically, Ye et al. (2004) found an increase in particle diameter with increasing Reynolds number, and Clark and Doering (2008) observed a parabolic relationship between the mean diameter and the dissipation rate, with the diameter increasing up to ~900 cm^2/s^3 and decreasing thereafter. All of the depth-averaged dissipation rates for this study fall below the value of ~900 cm^2/s^3 that Clark and Doering (2008) found to be the turning point between particle size increase and decrease. However, contrary to those results, the results of this study indicate a decrease of mean particle size with an increasing turbulent kinetic energy dissipation rate in this range. This discrepancy could be the result of several factors. One possibility is the limitation to the size of observable particles imposed by the imaging system. In the case of Ye et al. (2004) the image resolution was 0.25 to 0.30 mm/pixel, meaning no particles smaller than ~1.25 mm in diameter could be measured. For Clark and Doering (2006) the resolution was 0.055 mm/pixel, allowing for particles as small as 0.165 mm to be observed. Similarly, Clark and Doering (2008) reported a resolution of ~0.056 mm/pixel and a minimum particle size of ~0.2 mm. As mentioned previously, the resolution in the present study was ~0.0056 mm/pixel and the smallest observed particle was 0.022 mm in diameter. The absence of these small particles, which have previously been observed by Daly and Colbeck (1986), would drive up the overall average of the calculated size distributions in all cases but this would probably not be enough to reverse the trend.

A more likely possibility is that the size distribution is affected by the method in which turbulence is generated. It is possible that the propellers used to generate turbulence in this study caused larger particles to fracture more easily, either due to the increased turbulence near the propellers or through direct contact with the propellers themselves. This fracturing would cause many more small particles to form through secondary nucleation, reducing the overall average particle size. In comparison, the shear flow produced in the counter-rotating flume used by Clark and Doering (2008) and Ye et al. (2004) is much more similar to the process that produces turbulence in a natural river flow and could be a more accurate representation of the variations in frazil size that changing turbulence intensity produces. However, the only way to be certain is to perform similar measurements of both particle size and turbulence intensity in natural streams.

Table 2
Size distribution properties for the particle diameter at all three propeller speeds in the three intervals.

Segment	125 rpm			225 rpm			325 rpm		
	Mean (mm)	Standard deviation (mm)	Number of particles	Mean (mm)	Standard deviation (mm)	Number of particles	Mean (mm)	Standard deviation (mm)	Number of particles
Production	1.03	0.81	9638	0.80	0.64	6878	0.67	0.52	21,346
Peak	0.92	0.69	8304	0.64	0.47	10,795	0.56	0.38	27,551
Flocculation	0.85	0.63	6146	0.58	0.40	7480	0.57	0.43	79,457
Total	0.94	0.73	25,572	0.66	0.51	29,283	0.59	0.45	146,073

Table 3
Properties of the combined experimental data sets for each propeller speed, prior to particle flocculation.

Propeller speed (rpm)	Tank averaged ε (cm^2/s^3)	Number of experiments	Number of particles	Standard deviation (mm)	Mean (mm)
125	23.9	10	25,572	0.73	0.94
225	85.5	5	4143	0.71	0.75
325	335.6	12	19,374	0.54	0.66

7. Summary and conclusions

A series of experiments were conducted in which frazil ice particles were generated at different turbulence intensities and photographed under cross-polarised light in a laboratory frazil ice tank. The evolution of the frazil particle size distribution characteristics and numbers of suspended particles were studied throughout the supercooling process. It was found that the number of frazil particles initially increased quite rapidly and then decreased at a slower rate for the remainder of the experiment, as fewer particles were produced and existing particles were lost to flocculation or rose to the water surface. The mean particle size showed a similar trend although a near-equilibrium mean particle diameter was ultimately reached, at approximately the same time as the number of suspended particles peaked. This leads to the conclusion that larger particles may be more prone to form frazil flocs or fracture into smaller particles, thereby reducing the overall mean of the individual suspended particles. In addition, the growth of the remaining particles is halted due to a combination of an increased concentration of dissolved solids in the water, which depresses the freezing point, and an increase in water temperature. A lognormal distribution was found to offer a reasonable fit to the particle size distribution at all stages of the experiment. However, a secondary peak was observed at particle diameters of approximately 2 to 3 mm, which was very pronounced at the lower propeller speeds and the cause of this is unknown.

At each of the propeller speeds used to generate turbulence in the tank, ADV measurements were used to estimate a representative estimate of the overall turbulent kinetic energy dissipation rate. The mean particle sizes were 0.94, 0.75, and 0.66 mm and the corresponding values of the turbulent kinetic energy dissipation rate were 23.9, 85.5, and 336 cm^2/s^3, at propeller speeds of 125, 225, and 325 rpm, respectively. This trend of decreasing particle size with increasing dissipation rate is contrary to the results obtained in two previous studies. Therefore, a priority for future research should be to directly measure the frazil particle size and turbulence intensity in natural streams to determine how varying turbulence levels impact the particle size distribution.

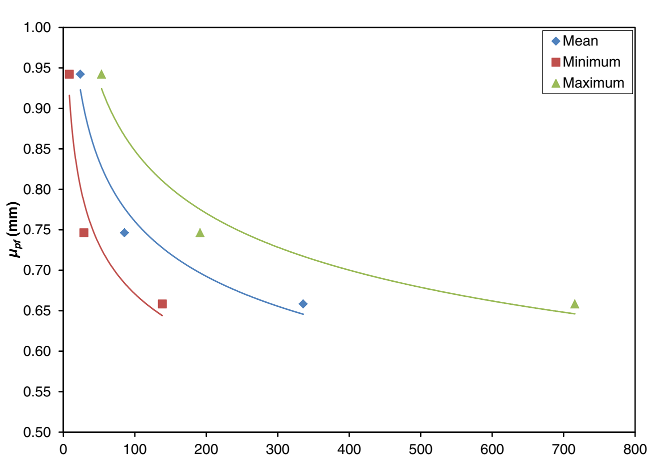

Fig. 11. Mean pre-flocculation particle diameter, μ_{pf}, plotted as a function of the depth-averaged turbulent kinetic energy dissipation rate, ε.

Acknowledgments

This research was supported by the Natural Sciences and Engineering Research Council of Canada (NSERC), which is gratefully acknowledged. We thank Perry Fedun and Chris Krath for providing technical assistance, Christine Hereygers and Drs. David Sego and Derek Martin for facilitating access to the Cold Room Facility, and Dr. Ali Habibzadeh for assistance processing the ADV data.

References

Brown, R.S., Hubert, W.A., Daly, S.F., 2011. A primer on winter, ice, and fish: what fisheries biologists should know about winter ice processes and stream-dwelling fish. Fisheries 36, 8–26. http://dx.doi.org/10.1577/03632415.2011.10389052.

Carstens, T., 1966. Experiments with supercooling and ice formation in flowing water. Geofys. Publ. 26, 1–18.

Clark, S., Doering, J., 2006. Laboratory experiments on frazil-size characteristics in a counterrotating flume. J. Hydraul. Eng. 132, 94–101. http://dx.doi.org/10.1061/(ASCE)0733-9429(2006)132:1(94).

Clark, S., Doering, J., 2008. Experimental investigation of the effects of turbulence intensity on frazil ice characteristics. Can. J. Civ. Eng. 35, 67–79. http://dx.doi.org/10.1139/L07-086.

Clark, S.P., Doering, J.C., 2009. Frazil flocculation and secondary nucleation in a counter-rotating flume. Cold Reg. Sci. Technol. 55, 221–229. http://dx.doi.org/10.1016/j.coldregions.2008.04.002.

Daly, S.F., 1984. Frazil Ice Dynamics. Hanover, N. H.

Daly, S.F., 1994. Report on Frazil Ice. Cold Regions Research & Engineering Laboratory, Hanover, N. H.

Daly, S.F., 2013. Frazil ice. In: Beltaos, S. (Ed.), River Ice Formation. Committee on River Ice Processes and the Environment, CGU-HS, Edmonton, Alberta, pp. 107–134.

Daly, S.F., Colbeck, S.C., 1986. Frazil ice measurements in CRREL's flume facility, Proceedings of the IAHR Ice Symposium 1986. International Association for Hydraulic Research, Iowa City, Iowa, USA pp. 427–438.

Doering, J.C., Morris, M.P., 2003. A digital image processing system to characterize frazil ice. Can. J. Civ. Eng. 30, 1.

Dubé, M., Turcotte, B., Morse, B., 2014. Inner structure of anchor ice and ice dams in steep channels. Cold Reg. Sci. Technol. 106–107, 194–206. http://dx.doi.org/10.1016/j.coldregions.2014.06.013.

Ettema, R., Karim, M.F., Kennedy, J.F., 1984. Laboratory experiments on frazil ice growth in supercooled water. Cold Reg. Sci. Technol. 10, 43–58. http://dx.doi.org/10.1016/0165-232X(84)90032-6.

Forest, T.W., 1986. Thermodynamic Stability of Frazil Ice Crystals, in: Proceedings of the Fifth International Offshore Mechanics and Arctic Engineering (OMAE) Symposium. The American Society of Mechanical Engineers, Tokyo, Japan pp. 266–270.

Forest, T.W., Sharma, R., 1992. Growth rates of frazil ice discs. Proceedings of the 11th International Symposium on Ice. International Association for Hydraulic Research, Banff, Alberta, pp. 723–734.

Ghobrial, T.R., Loewen, M.R., Hicks, F., 2012. Laboratory calibration of upward looking sonars for measuring suspended frazil ice concentration. Cold Reg. Sci. Technol. 70, 19–31. http://dx.doi.org/10.1016/j.coldregions.2011.08.010.

Ghobrial, T.R., Loewen, M.R., Hicks, F.E., 2013. Characterizing suspended frazil ice in rivers using upward looking sonars. Cold Reg. Sci. Technol. 86, 113–126. http://dx.doi.org/10.1016/j.coldregions.2012.10.002.

Gosink, J.P., Osterkamp, T.E., 1983. Measurements and analyses of velocity profiles and frazil Ice-crystal rise velocities during periods of frazil-ice formation in rivers. Ann. Glaciol. 79–84.

Hammar, L., Shen, H.T., 1995. Frazil evolution in channels. J. Hydraul. Res. 33, 291–306. http://dx.doi.org/10.1080/00221689509498572.

Islam, M.R., Zhu, D.Z., 2013. Kernel density-based algorithm for despiking ADV data. J. Hydraul. Eng. 139, 785–793. http://dx.doi.org/10.1061/(ASCE)HY.1943-7900-0000734.

Jasek, M., Ghobrial, T., Loewen, M., Hicks, F., 2011. Comparison of CRISSP modeled and SWIPS measured ice concentrations on the Peace River. Proceedings of the 16th Workshop on River Ice. CGU HS Committee on River Ice Processes and the Environment, Winnipeg, Manitoba, p. 25.

Kellerhals, R., Neill, C.R., Bray, D.I., 1972. Hydraulic and Geomorphic Characteristics of Rivers in Alberta. Alberta Cooperative Research Program in Highway and River Engineering. Edmonton, Alberta.

Marko, J.R., Jasek, M., Topham, D.R., 2015. Multifrequency analyses of 2011–2012 Peace River SWIPS frazil backscattering data. Cold Reg. Sci. Technol. 110, 102–119. http://dx.doi.org/10.1016/j.coldregions.2014.11.006.

McFarlane, V.J., 2014. Laboratory Studies of Suspended Frazil Ice Particles. University of Alberta.

McLelland, S.J., Nicholas, A.P., 2000. A new method for evaluating errors in high-frequency ADV measurements. Hydrol. Process. 14, 351–366. http://dx.doi.org/10.1002/(SICI)1099-1085(20000215)14:2<351::AID-HYP963>3.0.CO;2-K.

Morse, B., Richard, M., 2009. A field study of suspended frazil ice particles. Cold Reg. Sci. Technol. 55, 86–102. http://dx.doi.org/10.1016/j.coldregions.2008.03.004.

Osterkamp, T.E., 1978. Frazil ice formation: a review. J. Hydraul. Div. 104, 1239–1255.

Osterkamp, T.E., Gosink, J.P., 1983. Frazil ice formation and ice cover development in interior Alaska streams. Cold Reg. Sci. Technol. 8, 43–56.
Pope, S.B., 2000. Turbulent Flows. Cambridge University Press, Cambridge, U.K.
Pratt, W.K., 2007. Digital Image Processing, 4th Edition. John Wiley & Sons, Hoboken, NJ.
Richard, M., Morse, B., 2008. Multiple frazil ice blockages at a water intake in the St. Lawrence River. Cold Reg. Sci. Technol. 53, 131–149. http://dx.doi.org/10.1016/j.coldregions.2007.10.003.
Richard, M., Morse, B., Daly, S.F., Emond, J., 2011. Quantifying suspended frazil ice using multi-frequency underwater acoustic devices. River Res. Appl. 27, 1106–1117. http://dx.doi.org/10.1002/rra.1446.
Romagnoli, M., García, C.M., Lopardo, R.A., 2012. Signal postprocessing technique and uncertainty analysis of ADV turbulence measurements on free hydraulic jumps. J. Hydraul. Eng. 138, 353–357. http://dx.doi.org/10.1061/(ASCE)HY.1943-7900.0000507.
Stiansen, J.E., Sundby, S., 2001. Improved methods for generating and estimating turbulence in tanks suitable for fish larvae experiments. Sci. Mar. 65, 151–167. http://dx.doi.org/10.3989/scimar.2001.65n2151.
Stickler, M., Alfredsen, K.T., Linnansaari, T., Fjeldstad, H., 2010. The influence of dynamic ice formation on hydraulic heterogeneity in steep streams. River Res. Appl. 26, 1187–1197. http://dx.doi.org/10.1002/rra.1331.
Tennekes, H., Lumley, J.L., 1972. A First Course in Turbulence. MIT Press, Cambridge, Mass.
Tsang, G., Hanley, T.O., 1985. Frazil formation in water of different salinities and supercoolings. J. Glaciol. 31, 74–85.
Ye, S.Q., Doering, J., 2004. Simulation of the supercooling process and frazil evolution in turbulent flows. Can. J. Civ. Eng. 31, 915–926. http://dx.doi.org/10.1139/L04-055.
Ye, S.Q., Doering, J., Shen, H.T., 2004. A laboratory study of frazil evolution in a counter-rotating flume. Can. J. Civ. Eng. 31, 899–914.